Covalent Attachment of TAT Peptides and Thiolated Alkyl Molecules on GaAs Surfaces

Youngnam Cho[†] and Albena Ivanisevic*[,†,‡]

Department of Chemistry and Weldon School of Biomedical Engineering, Purdue University, West Lafayette, Indiana 47907

Received: March 28, 2005; In Final Form: May 12, 2005

Four TAT peptide fragments were used to functionalize GaAs surfaces by adsorption from solution. In addition, two well-studied alkylthiols, mercaptohexadecanoic acid (MHA) and 1-octadecanethiol (ODT) were utilized as references to understand the structure of the TAT peptide monolayer on GaAs. The different sequences of TAT peptides were employed in recognition experiments where a synthetic RNA sequence was tested to verify the specific interaction with the TAT peptide. The modified GaAs surfaces were characterized by atomic force microscopy (AFM), X-ray photoelectron spectroscopy (XPS), and Fourier transform infrared reflection absorption spectroscopy (FT-IRRAS). AFM studies were used to compare the surface roughness before and after functionalization. XPS allowed us to characterize the chemical composition of the GaAs surface and conclude that the monolayers composed of different sequences of peptides have similar surface chemistries. Finally, FT-IRRAS experiments enabled us to deduce that the TAT peptide monolayers have a fairly ordered and densely packed alkyl chain structure. The recognition experiments showed preferred interaction of the RNA sequence toward peptides with high arginine content.

Introduction

The importance of successfully modifying semiconductor materials with biomolecules has been identified by researchers working on novel diagnostic devices, molecular electronics, and sensing modalities. A number of studies have detailed the ability to control the properties of semiconductors such as electro- and photoluminescence by simply adsorbing molecules on such surfaces using rational chemical design criteria.[1] Publications have described the behaviors of a wealth of adsorbates on Si, Ge, CdSe, and other II−VI semiconductors, but relatively few reports exist on III−V materials. In particular, GaAs is of great interest because it allows flexible engineering of its band-gap properties, has high electron mobility, and can be utilized in traditional fabrication approaches. However, this material has been notoriously difficult to work with due to its chemical instability.[2] Furthermore, this instability is even harder to control under physiological conditions, which are necessary for surface modifications with a variety of biomolecules. Some systematic studies have been published that dealt with the direct attachment of thiol molecules to the bare GaAs surfaces.[3−6] These studies have established the possibility to form a covalent attachment to the surface if the native oxide layer is removed prior to the passivation with the thiol. Other efforts directed toward the attachment of biological molecules on these surfaces have focused on the adsorption of organic phosphates since they are fundamental building blocks of phospholipids and DNA.[7] Mohaddes-Ardabili et al. have shown that thiolated DNA molecules can be covalently anchored on GaAs and have utilized spectroscopy to show evidence that on an As-terminated surface both the thiol and the amine groups can be used to form an attachment.[8]

The literature on functionalization of GaAs to date has identified the major challenges in anchoring biomolecules and has demonstrated the need to show more examples of direct attachment of other classes of biomolecules as a step toward the utilization of this semiconductor in a variety of biomimetic platforms. Herein, we describe a strategy to anchor TAT peptides on GaAs as a step toward the utilization of this substrate in biorecognition sensors. The TAT protein is able to enter mammalian cells and activate their viral replication.[9,10] Short peptide sequences derived from this protein are called TAT peptides. Such peptides have received much attention due to their recognition properties, which are similar to those of the whole protein.[11] Recently, we showed that these peptides can be anchored on SiO_x and Au surfaces using adsorption from solution, microcontact printing, and dip-pen nanolithography.[12,13] In this paper, we describe the adsorption process of various sequences of synthetic TAT peptide fragments to GaAs surfaces. We also characterize the composition and structure of the monolayers and record their specific interaction with TAR RNA molecules. Two well-studied alkylthiols, 16-mercaptohexadecanoic acid (MHA) and 1-octadecanethiol (ODT), were chosen to compare with the structure of the peptide on GaAs substrates and contribute to a better understanding of the packing of the molecules on the surface. We characterize the composition and structure of the functionalized surfaces by atomic force microscopy (AFM), X-ray photoelectron spectroscopy (XPS), and Fourier transform infrared reflection absorption spectroscopy (FT-IRRAS). The experiments that we report demonstrate that synthetic peptides can be anchored directly on GaAs surfaces and their orientation and recognition properties show promise for incorporation in future sensing strategies.

Experimental Section

Reagents and Materials. The n-type GaAs (100) wafers doped with $(0.5-2) \times 10^{18}$ cm^{-3} Si were purchased from University Wafer (Boston, MA). The wafers were cut into

* Author to whom correspondence should be addressed. E-mail: albena@purdue.edu.
† Department of Chemistry.
‡ Weldon School of Biomedical Engineering.

10.1021/jp0515737 CCC: $30.25
Published on Web 06/10/2005

TABLE 1: Adsorbates Used for the GaAs Surface Functionalization

peptide A (15 aa)	H_2N-Cys-Gly-Ile-Ser-Tyr-Gly-**Arg**-Lys-Lys-**Arg**-**Arg**-Gln-**Arg**-**Arg**-**Arg**-OH
peptide B (7 aa)	H_2N-Cys-Gly-Ile-Ser-Tyr-Gly-**Arg**-OH
peptide C (10 aa)	H_2N-Cys-**Arg**-Lys-**Arg**-**Arg**-Gln-**Arg**-**Arg**-**Arg**-OH
peptide D (34 aa)	H_2N-Cys-Gly-Ile-Ser-Tyr-Gly-**Arg**-Lys-Lys-**Arg**-**Arg**-Gln-**Arg**-**Arg**-**Arg**-Pro-Pro-Gln-Gly-Ser-Gln-Thr-His-Gln-Val-Ser-Leu-Ser-Lys-Gln-Pro-Thr-Ser-Gln-OH
1-octadecanethiol (ODT)	$SH(CH_2)_{17}CH_3$
18-mercaptohexadecanoic acid (MHA)	$SH(CH_2)_{15}CO_2H$

smaller pieces (0.5×0.5 cm^2) and cleaned with acetone, pure ethanol, and deionized water and subsequently dried with N_2 gas. All GaAs substrates were etched with concentrated HCl for 1 min to remove the native oxide and provide an arsenic-covered surface. 16-Mercaptohexadecanoic acid (MHA), 90%, and 1-octadecanethiol (ODT), 98%, were purchased from Aldrich. Tris-EDTA buffer at pH ~8.0 and phosphate-buffered saline (PBS) at pH ~6.5 were obtained from Sigma. The four TAT peptide sequences (Table 1) containing an arginine-rich RNA-binding domain were synthesized by Bio-Synthesis (Lewisville, TX) where they were purified by HPLC and analyzed by MALDI-TOF. The TAR RNA sequence (5′-GGC CAG AUC UGA GCC UGG GAG CUC UCU GGC C-3′) and biotinylated TAR RNA were synthesized, purified, and analyzed by Integrated DNA Technologies (Coralville, IA). Biotin was attached at the 5′ end during the synthesis. Standard solid-phase chemistry protocols were used in both cases. 1.4-nm nanogold−streptavidin conjugates were purchased from Nanoprobe (Yaphank, NY) and diluted according to the manufacturer's instructions.

Surface Modification. Individual GaAs substrates of 0.5×0.5 cm^2 were incubated for 24 h at 4−8 °C in a 1 mM solution of each TAT peptide. All peptide solutions were prepared in PBS (pH ~6.5). After this treatment, the surfaces were rinsed several times with the same buffer, washed multiple times with ultrapure water, and dried under nitrogen. MHA and ODT were dissolved in absolute ethanol to obtain the desired concentrations, and the GaAs surfaces were immersed in a particular solution for 24−48 h. Subsequently, the surfaces were rinsed with ethanol and dried under nitrogen.

Recognition Experiments. The 5 μM solutions of TAR RNA and biotinylated TAR RNA were prepared in Tris-EDTA buffer at pH ~8.0. The 1.4-nm nanogold−streptavidin conjugates were diluted in the PBS buffer solution in a ratio of 1:5. GaAs surfaces functionalized with certain particular peptide sequences were incubated for 2−5 h at 4−8 °C in a 5 μM solution of biotinylated TAR RNA. Subsequently, these surfaces were rinsed with buffer and immersed in the diluted solution of nanogold−streptavidin for 1−2 h at 4−8 °C. After this treatment, the surfaces were rinsed several times with the same buffer, washed multiple times with ultrapure water, and dried under nitrogen.

Atomic Force Microscopy Characterization. A MultiMode Nanoscope IIIa from Digital Instruments, equipped with a Nanoscope software system, was used for AFM imaging. Single beam shaped tapping mode tips (model no. OMCL-AC16OTS-W2) were purchased from Veeco Instruments and had a spring constant of 42 N/m. All of the imaging experiments were performed under ambient conditions where the temperature and humidity ranged from 24 to 27 °C and 20% to 40%, respectively. Depending on the experimental conditions, the imaging was carried out with scan speeds of 2−4 Hz.

Contact Angle Measurements. The surface wetting properties were examined using a Tantac contact angle meter (model CAM-PLUS MICRO). All angles were read by the half-angle method. A drop of Milli-Q water (1 μL) was delivered to the surface using a syringe equipped with a micrometer. Static contact angle measurements were performed on at least three to five spots per sample. The standard deviation was calculated after the measurements were averaged.

Fourier Transform Infrared Reflection Absorption Spectroscopy. FT-IRRAS spectra were collected in the single-reflection mode with a FT-IR spectrometer (Thermo Nicolet, Madison, WI). This instrument was coupled to a Continuum IR microscope and equipped with a motorized XYZ translation stage. The p-polarized light was incident at 80° from the surface normal to the substrate. A narrow-band mercury cadmium telluride (MCT) detector was used to detect the reflected light. The spectrometer and the microscope unit were interfaced with a computer, which uses Thermo Nicolet's OMNIC software that provides all of the tools necessary for the FT-IRRAS analysis. Spectra were collected from 1024 scans at a resolution of 4 cm^{-1}. The water in the sample compartment was purged with high-purity nitrogen gas. An additional home-built chamber around the microscope unit was utilized to accomplish sufficient water exclusion. The data for the high- (2750−3100 cm^{-1}) and low-frequency regions (1500−1850 cm^{-1}) were acquired separately. All spectra of the monolayers formed by the adsorbates were subtracted from the spectra for the bare GaAs substrate. All samples used in the FT-IRRAS measurements were subsequently characterized by XPS.

X-Ray Photoelectron Spectroscopy. The XPS studies were done with a Kratos Axis ULTRA X-ray photoelectron spectrometer. The features of this instrument include a monochromatic Al Kα X-ray source, small-area extraction optics, a spherical capacitor electron energy analyzer, and a dual-channel plate-position-sensitive detector. Survey and high-resolution scans were collected for all samples discussed in this study. These scans were always collected from the same location on the sample. The pass energy was 160 eV when survey spectra were taken from 0 to 1100 eV. The pass energy was 40 eV when high-resolution scans were collected for each element of interest. The intensity obtained from the instrument was used to plot all XPS spectra. This was done to represent signal-to-noise ratios. The same *y*-axis scale is used in figures where the data are presented as stacks. A commercial software package, XPS PEAK (version 4.1) was used to do the data treatment. A mixture of Gaussian and Lorenzian functions was used to fit the peaks. A Shirley function was used to model the background.

Results and Discussion

Formation of Self-Assembled Monolayers on GaAs Surfaces. The various adsorbates utilized in this study are listed in Table 1. The four different peptides were chosen to vary in length. In addition, in peptide sequences A, C, and D the argenine-rich portion is located at different distances from the N-terminus. These three sequences are derived from the TAT protein. Peptide B was used as a control since it only contains one argentine and is the shortest sequence. Previous studies in the literature have focused on the importance of the basic amino acids in the sequence and have investigated their importance in recognition of specific RNA sequences as well as transduction ability.[14−16] The presence of a certain number of these basic

SCHEME 1: Summary of All the Surface Functionalization Steps

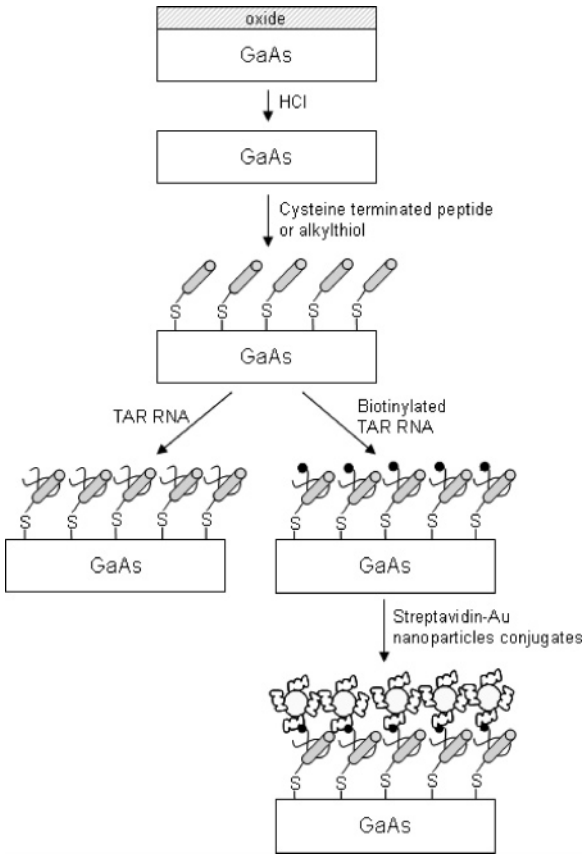

units has also been linked to the ability of the peptide to adopt an α-helical conformation.[17] The other two adsorbates listed in Table 1 are MHA and ODT, which were chosen because of their abilities to form well-ordered monolayers on GaAs[3] and metal surfaces.[18]

The various steps that we followed to functionalize the GaAs surfaces are shown in Scheme 1. We began the process by removing the native oxide layer that forms on the surface after storage. We experimented with variable treatment times during the HCl etch and concluded that the critical step leading to successful attachment is to place the freshly cleaned GaAs immediately in the adsorbate solution. In such cases, the most efficient attachment of the thiol groups to the arsenic-terminated surface was observed. RNA and biotylated RNA solutions were utilized to incubate the peptide-terminated surfaces for variable amounts of time in cases where recognition experiments were performed. In addition to the XPS experiments (see below), Au nanoparticles functionalized with streptavidin were used to test if the biotylated RNA is attached to the surface. We characterized the quality of the surface by AFM and contact angle measurements prior to evaluating the attachment steps in Scheme 1 via XPS and FT-IRRAS.

Tapping mode AFM measurements were done after functionalization with each adsorbate listed in Table 1. A summary of all of the AFM measurements is given in Table 2. The freshly etched GaAs showed a very smooth surface, a root-mean square of 0.18 ± 0.004 nm. The initial surface quality influences the subsequent quality of the monolayers that we produce by adsorption from solution. Upon the adsorption of ODT, MHA, and peptide A solutions, the surface roughness increased very little. Root-mean-square values of 0.36 ± 0.024, 0.44 ± 0.016, and 0.44 ± 0.037 nm were recorded for MHA-, ODT-, and peptide-A-terminated surfaces, respectively. On the basis of previous reports, we expect that thiol-containing molecules would attach to the GaAs surface through the sulfur. The fairly smooth surfaces, based on the roughness values, indicate that the monolayers composed of ODT, MHA, and the peptide molecules are considerably ordered structures. If the monolayers were disordered, then they are expected to form clusters of the molecules on the surface and thus result in a deterioration of the quality of the organized structures in the self-assembled monolayers (SAMs). After the recognition experiments with the RNA described in Scheme 1, the roughnesses of the peptide-terminated surfaces did not change significantly. However, upon the absorption of streptavidin-terminated gold particles, the roughnesses increased sharply to 1.20 ± 0.038 and 0.73 ± 0.019 nm for peptide-A- and peptide-B-terminated surfaces, respectively. These AFM roughness values favor the conclusion that the functionalized nanoparticles are attaching more specifically to the GaAs surface terminated with peptide A.

TABLE 2: Root-Mean-Square (rms) Values Determined by Tapping Mode AFM Measurements

surface	rms (nm)
as-received GaAs	0.31 ± 0.046
freshly etched GaAs	0.18 ± 0.004
GaAs + 1 mM MHA	0.44 ± 0.016
GaAs + 1 mM ODT	0.36 ± 0.024
GaAs + 1 mM peptide A	0.44 ± 0.037
GaAs + 1 mM peptide B	0.44 ± 0.019
GaAs + 1 mM peptide C	0.45 ± 0.028
GaAs + 1 mM peptide D	0.53 ± 0.023
GaAs + 1 mM peptide A + 5mM TAR RNA	0.41 ± 0.021
GaAs + 1 mM peptide B + 6 mM TAR RNA	0.41 ± 0.044
GaAs + 1 mM peptide C + 5 mM TAR RNA	0.44 ± 0.047
GaAs + 1 mM peptide D + 5 mM TAR RNA	0.44 ± 0.031
GaAs + 1 mM peptide A + 5 mM biotin−RNA	0.48 ± 0.127
GaAs + 1 mM peptide B + 5 mM biotin−RNA	0.46 ± 0.123
GaAs + 1 mM peptide A + 5 mM biotin−RNA + streptavidin−Au particles	1.20 ± 0.038
GaAs + 1 mM peptide B + 5 mM biotin−RNA + streptavidin−Au particles	0.73 ± 0.019

TABLE 3: Summary of Contact Angle Measurements

surface	angle (deg)
freshly etched GaAs	43 ± 5.8
GaAs + 1 mM MHA	50 ± 6.7
GaAs + 1 mM ODT	110 ± 1.2
GaAs + 1 mM peptide A	40 ± 1.5
GaAs + 1 mM peptide B	50 ± 2.4
GaAs + 1 mM peptide C	15 ± 5.2
GaAs + 1 mM peptide D	30 ± 8.3

The static contact angle measurements were carried out to observe the wettability of GaAs surfaces after exposure to the peptides and alkanethiol solutions, Table 3. The surfaces terminated with ODT monolayers exhibited high hydrophobicity while the MHA-modified surface showed a more hydrophilic nature. The trends in these contact angle measurements are consistent with those observed for monolayers on gold.[18] Monolayers formed by the series of TAT peptides had contact angles in the range of 15−50°. In all cases, we observed a difference in the wetting behavior between the freshly etched surface and the functionalized surface.

Surface Characterization by X-Ray Photoelectron Spectroscopy. XPS allowed us to examine the chemical composition of the GaAs surface after the various adsorption steps. Initially, we analyzed the following surfaces: as-received GaAs, freshly etched GaAs, and GaAs surfaces functionalized with the four peptides and the two alkanethiol molecules. To understand the composition of the surface, survey and high-resolution spectra

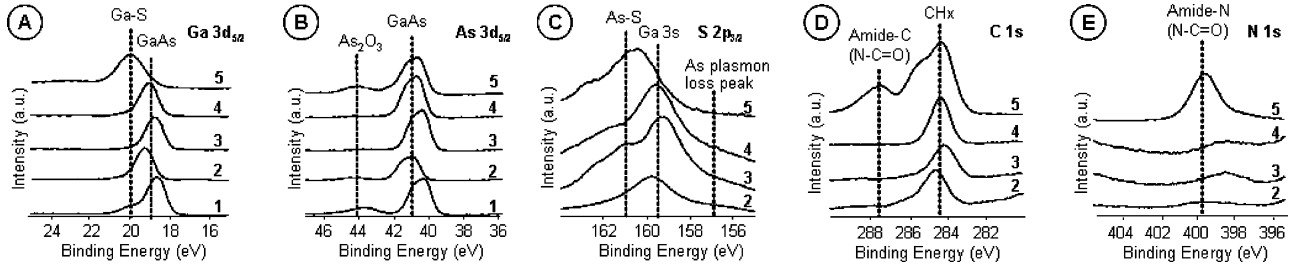

Figure 1. High-resolution XPS for (a) Ga 3d, (b) As 3d, (c) S 2p, (d) C 1s, and (d) N 1s regions on the following surfaces: (1) as-received GaAs, (2) freshly etched GaAs, (3) GaAs functionalized with MHA, (4) GaAs functionalized with ODT, and (5) GaAs functionalized with peptide A.

were collected. The survey spectra confirmed the presence of Ga 3d, As 3d, Ga 3s, C 1s, N 1s, S 2p, and O 1s on all modified surfaces. High-resolution spectra were recorded for the main core-level peaks of Ga 3d, As 3d, S 2p, C 1s, and N 1s because they enable one to evaluate the chemical structures of species present on the surface. Figure 1 shows the core-level high-resolution spectra of five different samples. From the Ga 3d and As 3d spectra, one can compare the as-received and freshly etched GaAs substrates. The data indicates that a lot of the native oxides were removed from the GaAs surface after immersion in the concentrated HCl. A small amount of the oxide peak is observed in the spectrum of the freshly etched surface resulting from either incomplete initial etching or the short storage before the XPS measurements. Examination of the same core-level spectra of Ga 3d and As 3d reveals the increased number of GaAs species on the cleaned substrate and on the surfaces functionalized with MHA and ODT. The predominant peak in the Ga 3d spectrum when the surface was functionalized with the peptide A molecule corresponds to Ga−S species at a binding energy of 20 eV.[19] The broad S 2p spectrum indicates the presence of an As plasmon loss peak, Ga 3s, and a As−S species on the surface.

The binding energy of a covalent bond between the sulfur and the surface is expected to be between 161.5 and 162.5 eV.[20−25] The existence of thiolated species (As−S) above 161.0 eV support the formation of a covalent bond after the adsorption of MHA, ODT, and TAT peptides on the surface. The thiolated surface is expected to prevent reoxidation and contamination on the surface. However, in the case of substrates functionalized by peptide solutions, a broad peak located at 163.1 eV was observed, indicating the presence of unbound sulfur on the GaAs surface or −S−S− species.[25] From the XPS results, one can confirm that the molecules are immobilized on the surface by a covalent bond through the sulfur. The high-resolution C 1s spectra reveal that the monolayers prepared from MHA and ODT solutions showed no differences when compared to a freshly etched surface. Cleaned substrates and ODT- and MHA-modified surfaces exhibit a single carbon peak centered at 284.0 eV. This peak indicates the presence of hydrocarbon chains on the surface. In the case of the peptide-functionalized surface, the high-resolution C 1s core-level spectra shows a distinctive peak centered at 284.2 eV. The peak can be deconvoluted and assigned to contain −C−N− species at 285.5 eV and amide C species at 287.4 eV. The presence of amides confirms the attachment of the peptides onto the surface. Moreover, the high-resolution N 1s core-level spectra also indicate the presence of NH_2 and amide N on surfaces modified with the peptides. The high-resolution analysis of the core-level spectra of the elements that we discussed so far suggests that molecules are on the surface and are anchored through sulfur to the GaAs. Table 4 provides a summary of the relative percentages of the various species comprising the Ga 3d, As 3d, S 2p, C 1s, and N 1s spectra on the different surfaces discussed in this section.

Surface Characterization by Fourier Transform Infrared Reflection Absorption Spectroscopy. FT-IRRAS was utilized to examine the chemical structure of the modified GaAs and understand the orientation and crystallinity of the adsorbed molecules on the surfaces. The peak position, intensity, and line shapes of the spectra enable one to confirm whether the monolayers composed of the various molecules are "liquidlike" or "crystallike" in nature. Prior to interpreting the reflection infrared spectra of the monolayers, we performed solution FT-IR experiments in the transmission mode. The solution IR experiments were done with all the adsorbates and are summarized in Figure 2. To interpret if the packing of the alkyl chains is liquidlike or crystallike, one looks at the peak positions of $\upsilon(CH_2)$ for direct evidence.[18,20,26−29] The symmetric and asymmetric CH_2 stretching modes are observed at 2924 and 2852, 2925 and 2853, and 2922−2923 and 2851−2852 cm^{-1}, in the solution FT-IR spectra of ODT, MHA, and peptide A, respectively. Since the low concentration of methyl group results in weak intensity, a small CH_3 C−H stretching band is observed in both the solution IR spectra of ODT and those of the four peptides. In the case of a crystallike state, the frequency of the $\upsilon_{as}(CH_2)$ band is positioned at 2920 cm^{-1} whereas the $\upsilon_s(CH_2)$ band is centered at 2850 cm^{-1}.[18,26] However, the assigned position of $\upsilon_{as}(CH_2)$ in the liquidlike state is at a higher frequency by 2−5 cm^{-1}, and the $\upsilon_s(CH_2)$ at a higher frequency by 2−3 cm^{-1} when compared to the crystallike state. The high-frequency region of our data gives information about the crystallinity of the alkyl chains. The low-frequency region can be used to explain the structure of the peptide in detail, such as the orientation of the amide modes as well as the nature of interchain hydrogen bonding. In the MHA spectrum, strong peaks were observed at 1827 and 1717 cm^{-1}, corresponding to the C═O stretching mode. For the peptide molecules, one of the most important peaks, the amide I band corresponding to the carbonyl stretching, is expected to appear in the range of 1600−1700 cm^{-1}, whereas the amide II band assigned to the N−H stretching is expected between 1500 and 1600 cm^{-1}.[30] Polypeptides with α-helical content exhibit a strong amide I peak at ∼1660 cm^{-1} and a medium-intensity amide II peak at ∼1550 cm^{-1} in the solution phase.[31] Previous studies have indicated that the examination of interchain hydrogen bonding can be divided into two distinctive regions: (i) interchain hydrogen bonding that occurs in the range of less than 1650 cm^{-1} for amide I band and ∼1550−1560 cm^{-1} for an amide II and (ii) non-hydrogen bonding that appears between 1650 and ∼1510 cm^{-1}.[32,33] Our solution IR data shows a slight blue shift of the amide I peak to ∼1668 cm^{-1} for all peptide sequences. This suggests an alternation in the secondary structure, which results after non-hydrogen bonding. In addition, the appearance of a strong and narrow amide II peak at ∼1520 cm^{-1} supports the non-hydrogen bonding between amide groups. These observations are in good agreement with published data on secondary amides in the solution phase. On the basis of these

TABLE 4: Summary of the XPS Binding Energy (BE in eV) Assignments for Ga 3d, As 3d, N 1s, C 1s, and S 2p after the GaAs Surface Was Etched with HCl and Subsequently Modified with MHA, ODT, and Peptides A, B, C, and D

surface	Ga 3d BE (%), assignments	As 3d BE (%), assignments	N 1s BE (%), assignments	C 1s BE (%), assignments	S 2p BE (%), assignments
as-received GaAs	18.6 (76.0), GaAs	40.3 (41.6), GaAs $3d_{5/2}$ 41.0 (39.1), GaAs $3d_{3/2}$ 43.8 (19.3), As_2O_3 $3d_{5/2}$	284.0 (100.0), CH_x		156.5 (6.9), as plasmon loss peak 159.4 (83.5), Ga 3s 161.9 (9.6), thiolated S−GaAs
clean GaAs	19.3 (100.0), GaAs	41.0 (67.7), GaAs $3d_{5/2}$ 41.8 (22.8), GaAs $3d_{3/2}$ 44.2 (9.5), As_2O_3 $3d_{5/2}$		284.5 (82.7), C−C 285.8 (17.3), CH_x	156.8 (8.5), as plasmon loss peak 159.8 (76.4), Ga 3s 163.0 (15.1), disulfide
GaAs + MHA	18.8 (96.1), GaAs 20.1 (3.9), Ga_20_3	40.5 (73.9), GaAs $3d_{5/2}$ 41.2 (22.1), GaAs $3d_{3/2}$		284.0 (77.3), C−C 285.2 (22.7), CH_x	156.2 (3.2), as plasmon loss peak 159.3 (74.0), Ga 3s 161.1 (7.7), Ga 3s 162.2 (11.2), thiolated S−GaAs 162.9 (3.9), disulfide
GaAs + ODT	19.1 (89.7), GaAs 19.8 (10.3), GaAs	40.9 (76.7), GaAs $3d_{5/2}$ 41.5 (23.3), GaAs $3d_{3/2}$		284.3 (100.0), C−C	156.8 (10.8), as plasmon loss peak 159.5 (64.0), Ga 3s 162.0 (25.2), thiolated S−GaAs
GaAs + peptide A	20.0 (100.0), Ga−S	41.5 (67.9), GaAs $3d_{5/2}$ 44.0 (32.1), As_2O_3 $3d_{5/2}$	397.5 (7.3), NH_2 399.1 (92.7) ,amide N	284.1 (54.8), C−C 285.5 (18.2), C−N 287.4 (26.1), amide C	160.4 (72.3), Ga 3s 162.5 (19.2), thiolated S−GaAs 163.1 (8.5), disulfide
GaAs + peptide B	18.7 (36.1), GaAs 20.1 (65.9), Ga_2O_3	40.6 (70.7), GaAs $3d_{5/2}$ 42.5 (11.1), As_2O_3 $3d_{5/2}$ 44.0 (11.1), As_2O_3 $3d_{5/2}$	397.4 (59.2), NH_2 399.1 (40.8), amide N	284.1 (54.8), C−C 285.5 (28.0), C−N 287.4 (17.2), amide C	159.3 (52.5), Ga 3s 160.8 (21.6), Ga 3s 162.1 (25.9), thiolated S−GaAs
GaAs + peptide C	18.4 (7.0), GaAs 20.0 (93.0), Ga−S	40.6 (42.4), GaAs $3d_{5/2}$ 42.0 (3.2), As−S 42.9 (16.2), As−S 44.0 (38.2), As_2O_3 $3d_{5/2}$	397.5 (24.0), NH_2 399.2 (76.0), amide N	284.3 (55.2), C−C 285.5 (18.8), C−N 287.5 (26.0), amide C	160.0 (6.7), Ga 3s 160.6 (73.2), Ga 3s 162.5 (20.1), thiolated S−GaAs
GaAs + peptide D	19.3 (81.0), GaAs 20.0 (19.0), Ga−S	41.1 (53.1), GaAs $3d_{3/2}$ 41.9 (13.8), GaAs $3d_{3/2}$ 42.1 (18.0), As−S 44.5 (15.1), As_2O_3 $3d_{3/2}$	398.3 (12.0), NH_2 400.2 (88.0), amide N	285.1 (48.0), C−C 286.4 (32.3), C−N 288.4 (19.7), amide C	156.8 (12.1), as plasmon loss peak 159.9 (62.0), Ga 3d 162.5 (25.9), thiolated S−GaAs

results, one can conclude that in solution the peptides are not likely to adopt a regular peptide fold with an α-helical conformation.

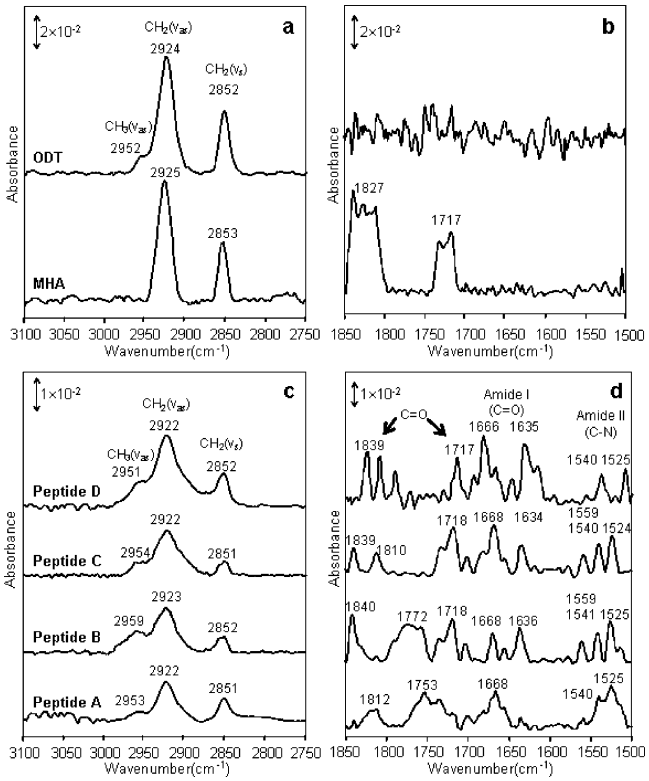

Figure 2. Solution FT-IR spectra of (a) the high-frequency region and (b) the low-frequency region of ODT and MHA and (c) the high-frequency region and (d) the low-frequency region for all peptides.

FT-IRRAS was used to evaluate the GaAs surface after the functionalization with each adsorbate, Figure 3. Surfaces modified with the ODT and MHA solutions exhibited peaks at 2916 and 2920 cm^{-1}, corresponding to $\upsilon_{as}(CH_2)$, whereas the

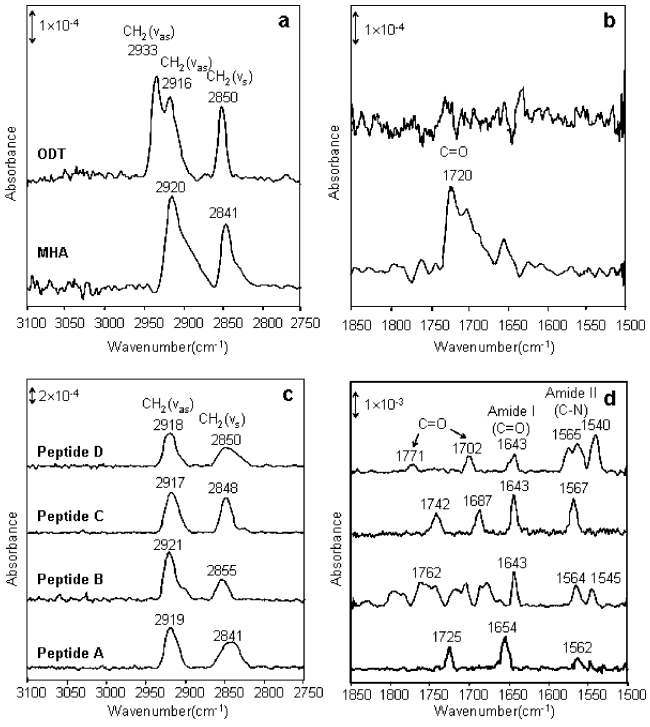

Figure 3. FT-IRRAS spectra of (a) the high-frequency region and (b) the low-frequency region of GaAs surfaces modified with ODT and MHA and (c) the high-frequency region and (d) the low-frequency region of GaAs surfaces functionalized with all four peptides.

$\upsilon_s(CH_2)$ was observed at 2850 and 2841 cm^{-1}, respectively. This observation indicates that the alkyl chains in our monolayer films are well-ordered and exhibit crystallike nature. Subsequently, we performed FT-IRRAS experiments with monolayers formed after the adsorption of the four peptides. On surfaces functionalized with peptides A, C, and D, the C−H peak positions shifted toward a lower frequency when compared to the solution FT-IR data. In the high-frequency regions, two strong methylene peaks were observed in the range of 2917−2919 and 2841−2850 cm^{-1}, where the former is assigned to an asymmetric stretching and the latter corresponds to the symmetric stretching of CH_2. In the case of surfaces functionalized with peptide B, the peaks for $\upsilon_{as}(CH_2)$ at 2921 cm^{-1} and $\upsilon_s(CH_2)$ at 2855 cm^{-1} shifted toward the higher-frequency region. A comparison of the data in Figure 3 with the solution FT-IR data suggests that the monolayers composed of peptides A, C, and D are densely packed and crystallike in structure. The monolayer composed of peptide B contains disordered alkyl chain packing. Previous studies indicate that alkanethiols in crystallike monolayers contain all-trans conformational order due to the effects of the high packing density.[18,21] The analysis of the low-frequency region is important to introduce further details with respect to the structure of the peptides on the surface. On the basis of the peak position and shape, the presence of interchain hydrogen bonding as well as the orientation of amide moiety can be deduced. GaAs surfaces modified with the four peptides displayed strong amide I peaks at 1643 and 1654 cm^{-1}, which is consistent with the presence of polypeptides with α-helical structure.[31] The amide I peak indicates the presence of interchain hydrogen bonding in the peptide monolayer although some alternation is expected due to the interaction between the peptide and the surface. In our experiments, amide II peaks were recorded at ∼1540 and ∼1560 cm^{-1}. The observation of an amide II peak supports the presence of hydrogen bonding in the monolayers composed of each peptide that we investigated. The shift toward higher frequency (from ∼1520 to ∼1560 cm^{-1}) as compared to the solution data agrees with the fact that the presence of hydrogen bonding is associated with the increased restriction on N−H bending. Taken in sum, the FT-IRRAS results suggest that the monolayers of the four different peptides have well-ordered, tightly packed alkyl chains that exhibit interchain hydrogen bonding.

Characterization of the Interactions between Peptide-Functionalized Surfaces and TAR RNA. TAT peptides are known to interact specifically with TAR RNA through their arginine-rich region (residues 49−59). This mechanism of interaction is still not clear and under investigation. Previously, researchers have used acoustic wave sensors to monitor and quantify this interation.[34] Peptide A is the exact same sequence used in previous experiments. Surfaces functionalized with each peptide were incubated in the TAR RNA solution. XPS revealed an increase in the C/N ratio for each surface terminated with a different peptide, Table 5. In addition, the C 1s and N 1s data was deconvoluted. On the basis of the N 1s spectrum, only the surfaces terminated with peptide A showed predominantly N−C═O species after incubation in the TAR RNA solution. We adapted streptavidin−biotin chemistry to better understand the specificity of RNA binding. The steps that we followed were first introduced when Scheme 1 was discussed. We performed some initial AFM evaluation of these surfaces, which was discussed above. First, we examined the binding of biotinylated TAR RNA to the immobilized peptides. Subsequently, streptavidin−gold particle conjugates were adsorbed onto the same surfaces. Since the interaction between streptavidin and biotin is very strong, the attachment of streptavidin-functionalized gold nanoparticles to the biotinylated RNA would indicate a specific binding between the TAR RNA and the peptide sequence. For proof-of-concept experiments, we chose surfaces terminated with peptides A and B. Peptide A has six arginine residues, and peptide B has only one arginine residue. Under physiological conditions, the TAT peptides are expected to become highly cationic because almost all amino acids are expected to be protonated.

TABLE 5: Summary of the XPS Binding Energy (BE in eV) Assignments for N 1s and C 1s after Functionalization with the Different Peptides and Subsequent Incubation in RNA Solution

surface	N 1s BE (%), assignments	C 1s BE (%), assignments	C/N ratio
peptide A	397.5 (7.3), NH_2 399.1 (92.7), amide N	284.2 (55.7), C−C 285.5 (18.2), C−N 287.4 (26.1), amide C	1.36
peptide B	397.4 (59.2), NH_2 399.1 (40.8), amide N	284.1 (54.8), C−C 285.5 (28.0), C−N 287.4 (17.2), amide C	1.61
peptide C	397.5 (24.0), NH_2 399.2 (76.0), amide N	284.3 (55.2), C−C 285.5 (18.8), C−N 287.5 (26.0), amide C	1.12
peptide D	398.3 (12.0), NH_2 400.2 (88.0), amide N	285.1 (48.0), C−C 286.3 (32.3), C−N 288.4 (19.7), amide C	2.08
peptide A + RNA	399.8 (100.0), amide N	285.0 (45.8), C−C 286.6 (42.4), C−N 288.2 (11.8), amide C	2.25
peptide B + RNA	397.8 (29.0), NH_2 399.3 (71.0), amide N	284.1 (58.0), C−C 285.5 (32.0), C−N 287.5 (10.0), amide C	3.40
peptide C + RNA	398.0 (20.0), NH_2 399.4 (80.0), amide N	284.4 (38.1), C−C 285.9 (47.9), C−N 287.6 (14.0), amide C	2.17
peptide D + RNA	398.0 (20.8), NH_2 399.3 (79.2), amide N	284.3 (50.3), C−C 285.5 (31.2), C−N 287.5 (18.5), amide C	2.56

We analyzed the surfaces by XPS after the gold nanoparticles were adsorbed. Surfaces that were initially functionalized with peptide A displayed binding energies at 85.5 and 89.2 eV. For bulk gold, these binding energies are expected at 84.0 and 87.7 eV. GaAs surfaces initially functionalized with peptide B were evaluated after the gold nanoparticles adsorption and showed peaks at 83.8 and 87.5 eV, corresponding to the presence of gold. From the relaxation model, it is notable that the core-level binding energies of isolated species such as an atom or a small cluster will be larger than that of the bulk metal.[35−37] In the bulk metal where the hole created during the photoionization is shielded by neighboring atoms, the energy of the final state becomes lower. This can be understood by the lower coordination number of the surface atoms. Consequently, the bulk metal will have a lower binding energy due to this effect. In the case of isolated atoms, one cannot expect this phenomenon, and a positive shift in the binding energies for gold will be observed. On the basis of this model and the XPS data acquired, the aggregation of gold nanoparticles induced by nonspecific interactions occurs on surfaces functionalized with peptide B. On surfaces terminated with peptide A, the gold nanoparticles are not aggregating due to their specific interaction with the biotin on the RNA and the presence of the streptavidin moieties. AFM studies on the two types of surfaces support the XPS conclusions. However, we plan to perform experiments with

lithographic patterns composed of different peptides to confirm this hypothesis.

Conclusions

In this paper, we demonstrate the following: (i) GaAs surfaces were modified by adsorption from solution with four different peptide sequences and two well-known alkylthiols, MHA and ODT. (ii) XPS was used to show that surfaces modified with various peptide sequences exhibit similar surface chemistry and homogeneity. (iii) FT-IRRAS data allowed the evaluation of the crystallinity of the modified surfaces. The FT-IRRAS results indicated that the peptides and alkanethiol monolayers exhibit crystallike or well-ordered packing on the GaAs substrates. (iv) Experiments with RNA, biotinylated RNA, and functionalized gold nanoparticles showed that after the peptides are anchored on the GaAs surface they retain their biorecognition properties.

Acknowledgment. This work was supported by the Bindley Biosciences Center at Purdue University and by the National Aeronautics and Space Administration (NASA) under Award No. NCC 2-1363. Any opinions, findings, and conclusions expressed in this material are those of the authors and do not necessarily reflect the views of NASA. The authors acknowledge experimental help from Dr. Richard Haasch (University of Illinois at Urbana−Champaign (UIUC)) to carry out the XPS characterization. All XPS experiments were performed at the Center for Microanalysis of Materials, UIUC, which is partially supported by U. S. Department of Energy under Grant No. DEFG02-96-ER45439.

References and Notes

(1) Seker, F.; Meeker, K.; Kuech, T. F.; Ellis, A. B. *Chem. Rev.* **2000**, *100*, 2505−2536.

(2) Ye, S.; Li, G.; Noda, H.; Uosaki, K.; Osawa, M. *Surf. Sci.* **2003**, *529*, 163−170.

(3) Sheen, C. W.; Shi, J. X.; Martensson, J.; Parikh, A. N.; Allara, D. L. *J. Am. Chem. Soc.* **1992**, *114*, 1514−1515.

(4) Shaporenko, A.; Adlkofer, K.; Johansson, L. S. O.; Ulman, A.; Grunze, M.; Tanaka, M.; Zharnikov, M. *J. Phy. Chem. B* **2004**, *108*, 17964−17972.

(5) Shaporenko, A.; Adlkofer, K.; Johansson, L. S.; Tanaka, M.; Zharnikov, M. *Langmuir* **2003**, *19*, 4992−4998.

(6) Adlkofer, K.; Eck, W.; Grunze, M.; Tanaka, M. *J. Phys. Chem. B* **2003**, *107*, 587−591.

(7) Artzi, R.; Daube, S. S.; Cohen, H.; Naaman, R. *Langmuir* **2003**, *19*, 7392−7398.

(8) Mohaddes-Ardabili, L.; Martinez-Miranda, L. J.; Silverman, J.; Christou, A.; Salamanca-Riba, L. G.; Al-Sheikhly, M.; Bentley, W. E.; Ohuchi, F. *Appl. Phys. Lett.* **2003**, *83*, 192−194.

(9) Fawell, S.; Seery, J.; Daikh, Y.; Moore, C.; Chen, L. L.; Pepinsky, B.; Barsoum, J. *Proc. Natl. Acad. Sci. U.S.A.* **1994**, *91*, 664−668.

(10) Long, K. S.; Crothers, D. M. *Biochemistry* **1995**, *34*, 8885−8895.

(11) Kimura-Suda, H.; Petrovykh, D. Y.; Tarlov, M. J.; Whitman, L. J. *J. Am. Chem. Soc.* **2003**, *125*, 9014−9015.

(12) Cho, Y.; Ivanisevic, A. *J. Phy. Chem. B* **2004**, *108*, 15223−15228.

(13) Cho, Y.; Ivanisevic, A. *J. Phy. Chem. B* **2005**, *109*, 6225−6232.

(14) Zhao, M.; Kircher, M. F.; Josephson, L.; Weissleder, R. *Bioconjugate Chem.* **2002**, *13*, 840−844.

(15) Zhao, M.; Weissleder, R. *Med. Res. Rev.* **2004**, *24*, 1−12.

(16) Snyder, E. L.; Dowdy, S. F. *Pharm. Res.* **2004**, *21*, 389−393.

(17) Torchilin, V. P.; Rammohan, R.; Weissig, V.; Levchenko, T. S. *Proc. Natl. Acad. Sci. U.S.A.* **2001**, *98*, 8786−8791.

(18) Nuzzo, R. G.; Dubois, L. H.; Allara, D. L. *J. Am. Chem. Soc.* **1990**, *112*, 558−569.

(19) Yang, G. H.; Zhang, Y.; Kang, E. T.; Neoh, K. G.; Huang, W.; Teng, J. H. *J. Phys. Chem. B* **2003**, *107*, 8592−8598.

(20) Li, Z.; Chang, S. C.; Williams, R. S. *Langmuir* **2003**, *19*, 6744−6749.

(21) Laibins, P. E.; Whitesides, G. M.; Allara, D. L.; Tao, Y. T.; Parikh, A. N.; Nuzzo, R. G. *J. Am. Chem. Soc.* **1991**, *113*, 7152−7167.

(22) Petrovykh, D. Y.; Kimura-Suda, H.; Whitman, L. J.; Tarlov, M. J. *J. Am. Chem. Soc.* **2003**, *125*, 5219−5226.

(23) Winter, R.; Nixon, P. G.; Gard, G. L.; Graham, D. J.; Castner, D. G.; Holcomb, N. R.; Grainger, D. W. *Langmuir* **2004**, *20*, 5776−5781.

(24) Yam, C.-M.; Pradier, C.-M.; Salmain, M.; Marcus, P.; Jaouen, G. *J. Colloid Interface Sci.* **2001**, *235*, 183−189.

(25) Love, J. C.; Wolfe, D. B.; Haasch, R.; Chabinyc, M. L.; Paul, K. E.; Whitesides, G. M.; Nuzzo, R. G. *J. Am. Chem. Soc.* **2003**, *125*, 2597−2609.

(26) Nakano, K.; Sato, T.; Tazaki, M.; Takagi, M. *Langmuir* **2000**, *16*, 2225−2229.

(27) Pardo, L.; Wilson, W. C.; Boland, T. *Langmuir* **2003**, *19*, 1462−1466.

(28) Azzam, W.; Wehner, B. I.; Fischer, R. A.; Terfort, A.; Woll, C. *Langmuir* **2002**, *18*, 7766−7769.

(29) Jennings, G. K.; Yong, T.-H.; Munro, J. C.; Laibinis, P. E. *J. Am. Chem. Soc.* **2003**, *125*, 2950−2957.

(30) Pradier, C.-M.; Salmain, M.; Liu, Z.; Methivier, C. *Surf. Interface Anal.* **2002**, *34*, 67−71.

(31) Enander, K.; Aili, D.; Baltzer, L.; Lundstrom, I.; Liedberg, B. *Langmuir* **2005**, *21*, 2480−2487.

(32) Clegg, R. S.; Hutchison, J. E. *Langmuir* **1996**, *12*, 5239−5243.

(33) Tam-Chang, S.-W.; Biebuyck, H. A.; Whitesides, G. M.; Jeon, N.; Nuzzo, R. G. *Langmuir* **1995**, *11*, 4371−4382.

(34) Tassew, N.; Thompson, M. *Anal. Chem.* **2002**, *74*, 5313−5320.

(35) Mason, M. G. *Phys. Rev. B* **1983**, *27*, 748−762.

(36) Radnik, J.; Mohr, C.; Claus, P. *Phys. Chem. Chem. Phys.* **2003**, *5*, 172−177.

(37) Cuenya, B. R.; Baeck, S. H.; Jaramillo, T. F.; McFarland, E. W. *J. Am. Chem. Soc.* **2003**, *125*, 12928−12934.